J. Fluid Mech. (1999), *vol.* 380, *pp.* 233–255. Printed in the United Kingdom

Mechanism for drop formation on a coated vertical fibre

By HSUEH-CHIA CHANG AND EVGENY A. DEMEKHIN†

Department of Chemical Engineering, University of Notre Dame, Notre Dame, IN 46556, USA

(Received 13 February 1997 and in revised form 10 September 1998)

Rayleigh instability on an axisymmetric viscous film around a vertical fibre produces localized wave structures (pulses) on a flat substrate film that can grow by an order of magnitude to form large capillary drops. We show that this drop formation process is driven by a unique mechanism in the form of an ever-growing pulse which leaves behind a trailing film thinner than the one it advances into. In addition to accumulating liquid from the film, the growing pulse also captures smaller and slower pulses in coalescence cascades. We construct this supercritical growing pulse by matched asymptotics and show that it will eventually evolve into a capillary drop if the local film thickness h is larger than $h_c = 1.68R^3H^{-2}$ where R is the fibre radius and H the capillary length. We also show that subcritical pulses with $h < h_c$ will equilibrate into stationary pulses that do not grow or coalesce readily to form drops.

1. Introduction

A unique hydrodynamic instability, about which our understanding has advanced beyond linear theory for wave inception to strongly nonlinear largetime dynamics, is the Rayleigh instability for an annular film on a vertical fibre. If the thickness of the film is small compared to the fibre radius, a leading-order long-wave evolution equation can be derived to replace the far more complex equations of motion (Trifonov 1992; Frenkel 1992). Theoretical and numerical analyses of this equation (Kalliadasis & Chang 1994*a*; Kerchman & Frenkel 1994) have focused on a curious experimental observation by Quere (1990) on the large-time asymptotic dynamics of this instability. Quere observes that, if the initial film thickness h_0 exceeds a critical value, small-amplitude waves on the film around a thin fibre can form large capillary drops of the dimension of the capillary length $H = (\sigma/\rho g)^{1/2}$ which are at least one order of magnitude larger than the former waves.

Kalliadasis & Chang (1994*a*) have constructed lone stationary pulses that travel steadily at constant speeds on a substrate of thickness h. They correspond to equilibrium states that isolated pulses can evolve into. They find that such equilibrium pulses can only exist for h less than

$$h_c = 1.68R^3/H^2, \tag{1}$$

where R is the fibre radius.

Both Kerchman & Frenkel (1994) and Kalliadasis & Chang (1994*a*) have carried out simulations on an extended domain with random initial conditions on an initial

† Permanent address: Department of Applied Mathematics, Kuban State Technological University, Krasnodar, 350072, Russia.

flat film of thickness h_0. The wave dynamics are also observed to be fundamentally different depending on the relative magnitude of h_0 and h_c. In both cases, the non-stationary, small-amplitude waves at inception evolve into well-separated pulses on a thin substrate film. This pulse formation mechanism is not understood but one scenario has been analysed by Chang *et al.* (1997). Once formed, however, the dynamics of each pulse seem to be determined only by the local substrate thickness h. A subcritical pulse ($h < h_c$) would equilibrate into one of the stationary pulses constructed by Kalliadasis & Chang. This equilibration can involve collecting fluid from the substrate or draining fluid from the pulse but the amplitude and speed of an isolate pulsed would eventually become stationary. The pulses may continue to interact weakly with their neighbours and adjust their spacing. However, extensive simulations show that coalescence rarely occurs after the subcritical pulses are formed. In the absence of coalescence and individual pulse growth, these subcritical pulses do not grow into drops.

This scenario is drammatically different for supercritical pulses with $h > h_c$. These pulses grow individually by collecting fluid from the substrate. Moreover, their growth rate is very different such that the larger pulses are much faster than the smaller ones. As a result, a large pulse eventually overtakes and captures its smaller and slower front neighbour in a coalescence event. The former pulse gains more fluid in the process and becomes even larger and faster. An entire train of smaller pulses can then be captured successively in a coalescence cascade by a trailing large pulse. This large pulse grows with each coalescence and continues to collect fluid from the substrate between coalescence events. Although the simulations cannot be carried out indefinitely and the model equation breaks down eventually when the growing pulses become too large, this combination of coalescence and individual growth is expected to drive the large supercritical pulses into drops.

We explore the distinctively different dynamics of subcritical and supercritical pulses here. In § 2, we carry out additional coalescence simulations to focus on the importance of continual fluid accumulation from the substrate film by the driving pulse. We then demonstrate in § 3 that such collection cannot be sustained under subcritical conditions by showing that isolated subcritical pulses will evolve into the stable stationary pulses of Kaliadasis & Chang. The spectral stability theory for the stationary pulses also allows us to determine their equilibration rate and quantify the reluctance of subcritical pulses to coalesce. We construct an asymptotic state for a supercritical pulse in § 4 that grows in a rapid self-similar $(t_* - t)^{-2}$ manner. This finite-time blow-up growth dynamics fuels the driving pulse in a coalescence cascade. Although (1) is favourably compared to Quere's measured critical film thickness in Kalliadasis & Chang (1994*a*), the critical h from §§2 and 3 is for the substrate beneath a developed pulse while Quere only measured the thickness of the initial waveless film. We reconcile this difference in §5 by estimating substrate drainage.

2. Pulse coalescence dynamics

We shall utilize the leading-order evolution equation derived by Trifonov (1992) and Frenkel (1992) for $(h_0/R) << 1$:

$$\frac{\partial h}{\partial t} + \frac{\partial}{\partial x}\left[\delta h^3\left(\frac{\partial^3 h}{\partial x^3} + \frac{\partial h}{\partial x}\right) + \tfrac{2}{3}h^3\right] = 0, \tag{2}$$

where

$$\delta = (2\sigma h_0/3\rho\, g\, R^3) = (2H^2 h_0/3R^3)$$

measures the ratio of curvature-driven flow of the Rayleigh instability to the gravity-driven mean flow. The film thickness h_0 is taken to be that of the initial waveless film and it has been used to scale the interfacial height. The fibre radius R is used to scale the axial coordinate x and the characteristic time used is R/U where $U = (gh_0^2/2\nu)$ is the interfacial velocity of the film. As a result of the scaling, the thickness of the initial waveless film is always unity. The critical condition $h_0 = h_c$ now corresponds to a critical $\delta_* = 1.12$. It is sometimes convenient to present the graphics in a frame moving with speed c and the equation in that frame becomes

$$\frac{\partial h}{\partial t} + \frac{\partial}{\partial x}\left[\delta h^3\left(\frac{\partial^3 h}{\partial x^3} + \frac{\partial h}{\partial x}\right) + \tfrac{2}{3}h^3 - ch\right] = 0. \tag{3}$$

Typically, c is chosen to be the pulse speed of an equilibrium subcritical pulse at the particular value of δ. It is hence well-defined only for subcritical values of δ, $\delta < \delta_*$.

We have developed a high-order finite-difference scheme similar to the one used in Chang *et al.* (1997) for falling film waves. A detailed description of the numerical method can be found in the references of that paper. For the current problem, (2) and (3) are integrated in time using 2000 spatial gridpoints. To minimize numerical error, 'soft' boundary conditions with vanishing first and second derivatives are often used at the two boundaries of large domains instead of periodic boundary conditions which are used for smaller domains. These soft conditions introduce a filtering effect on any wave propagating across the boundaries and wave dynamics that reach the boundaries must hence be ignored. To ensure the pertinent dynamics is captured before they reach the boundaries, very large domains exceeding 20 pulse widths are used with the soft boundary conditions. Such large computational domains introduce excessively high storage requirements, however, and we do not record the computed result for every time step. The graphical outputs often show some fluctuations due to this insufficient reporting of the computed result – they are not due to numerical error.

In figure 1, we depict the simulated interfacial profiles from (3) in a periodic domain of length 20π beginning with a small-amplitude ($< 10^{-3}$), zero-mean, random disturbance to $h_0 = 1$ at the supercritical condition of $\delta = 3$. As is evident, the profiles evolve through the linear filtering stage and heavily modulated sinuous waves are for roughly the wavelength λ of the fastest-growing mode from linear theory, $\lambda = 2\sqrt{2}\pi$. The modulation annihilates certain wave peaks at this stage to yield about six distinct wave crests. These fluctuating crests seem to phase lock and saturate for some time at about $h = 1.2$ before they slowly blossom individually into distinct pulses by $t = 10$ with h in excess of 2. These pulses possess the signature front dimple of capillary film flows (Wilson 1982; Wilson & Jones 1983; Hammond 1983). They are also separated by thin flat substrate films. Although the pulses are similar in shape, there are variations in their speed, height and separation which are legacies of the earlier modulations. As seen by comparing figures 1(*b*) and 1(*c*), isolated pulses continue to grow by accumulating fluid from the substrate. Well-packed pulses do not grow appreciably, presumably because of the limited reservoir of fluid in the substrate between pulses. The larger pulses travel faster and begin to encroach on the smaller ones in front. By $t = 15$, the largest one has coalesced with its front neighbour to induce a jump in its amplitude.

We follow the amplitude of this large pulse in figure 2(*a*). Its solitary growth prior

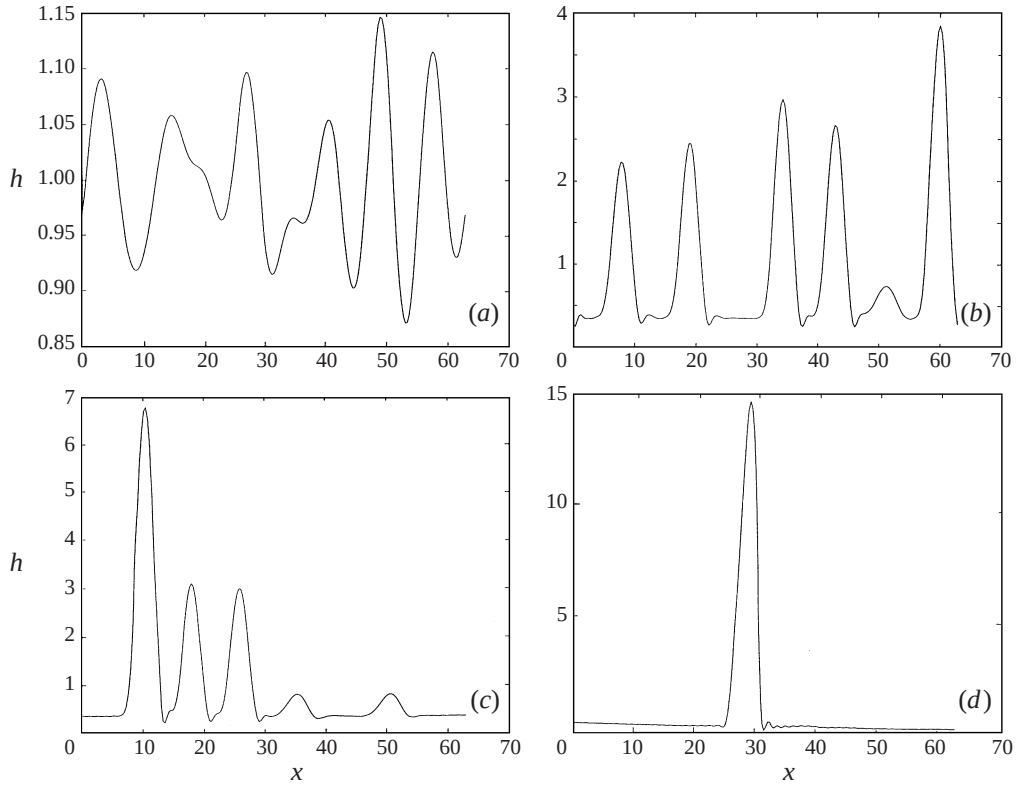

FIGURE 1. Simulated coalescence cascade with random initial condition at $\delta = 3$ and (*a*) $t = 2$, (*b*) 15, (*c*) 23 and (*d*) 30.

to the first coalescence is apparent and we see that it successively captures all five other pulses in due time, the last two in one violent gulp at $t = 24$, to form a monster pulse of amplitude 10. We also note that the large pulse either retains its amplitude or actually grows between coalescence events. The final lone pulse smooths the substrate and continues to grow, albeit more slowly, by collecting liquid from the substrate, as is evident from the amplitude growth beyond $t = 24$ in figure 2(*a*). Although it is not evident in figure 2(*a*), its amplitude eventually saturates at about 15, a full order of magnitude larger than the initial quasi-saturated waves at $t = 5$. This monster pulse stops growing when the substrate thickness reaches a critical value. The saturation occurs because we use a periodic computation domain with a finite amount of liquid. In an extended domain, the substrate beneath a supercritical pulse does not thin appreciably and the practically infinite reservoir of fluid allows the pulse to evolve into a drop. We shall demonstrate this in a later section.

It is questionable whether the long-wave expansion assumed in deriving (3) remains valid for the final large structures. We examine this in the Appendix by using a higher-order evolution equation and show that the drop formation mechanism offered by (3) remains valid for thin fibres whose radii are much smaller than the capillary length H.

To demonstrate that the large supercritical pulse continually accumulates fluid from the substrate film during the coalescence cascade, we track the substrate thickness χ behind the large pulse as a function of time in figure 2(*b*). It is clear that χ decreases

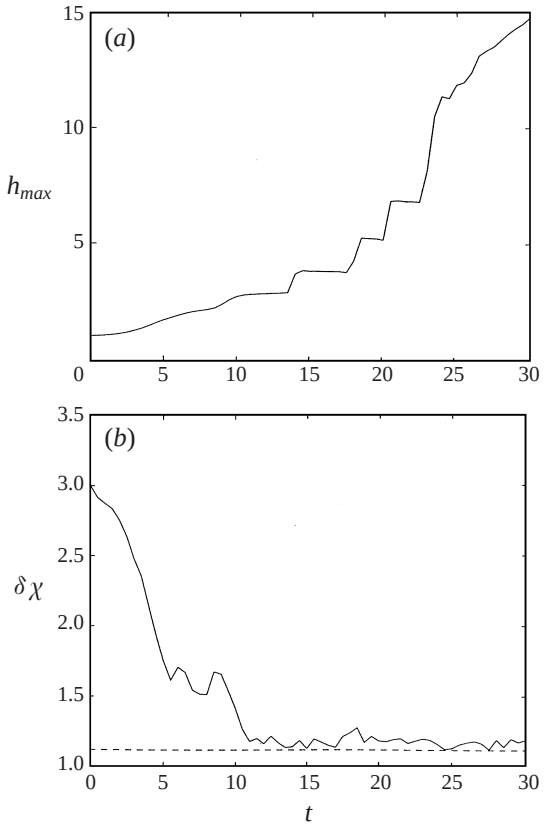

FIGURE 2. (*a*) Amplitude and (*b*) trailing substrate thickness χ of the large driving pulse in figure 1.

monotonically until $\chi\delta$ approaches the critical value δ_*. Since the substrate thins and its thickness decreases from its initial value of unity to χ, the effective δ for the growing pulse, based on its own substrate thickness, is not the original δ but $\delta\chi$. Figure 2(*b*) then suggests that the pulse ceases to grow under subcritical conditions $\delta < \delta_*$. We also note that χ has reached its asymptotic value by $t = 15$ while the pulse is still growing at $t = 25$. This suggests that the substrate thickness in front of the growing pulse is larger than χ and the jump in the substrate thickness across the pulse fuels the growth.

The scenario is completely different for subcritical conditions $\delta < \delta_*$. Extensive simulations by Kerchman & Frenkel (1994) and Kalliadasis & Chang (1994*a*) with random initial conditions have shown that subcritical pulses rarely coalesce. In figure 3, we have placed two subcritical pulses next to each other for $\delta = 0.8$. The front one is an equilibrium stationary pulse constructed by Kalliadasis & Chang (1994*a*) while the back one is larger with an amplitude 1.265 times the equilibrium value. It is clear that the two pulses interact with each other but there is no coalescence at the end. The back pulse drains its excess fluid and equilibrates by slowing down to a stationary pulse in the moving frame of figure 3. The front pulse gains some fluid during the interaction and moves forward. Although it is not shown in figure 3, the front pulse will also shed its excess fluid and equilibrate.

While the separation and amplitude variation in figure 3 are typical of the 'natural' conditions with random, small-amplitude initial conditions, one can force coalescence

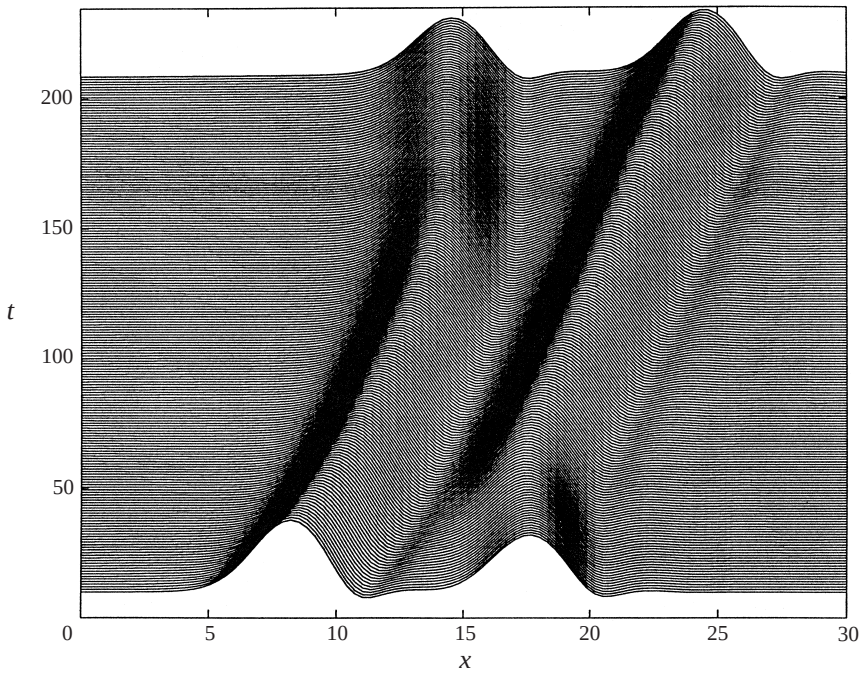

FIGURE 3. A subcritical equilibrium pulse at $\delta = 0.8$ followed by a larger pulse with 1.265 the equilibrium amplitude. The initial separation is $\Delta x = 10$.

of subcritical pulses by using extremely large and unnatural pulses. We place a pulse twice as large as the stationary in front of a train of equilibrium pulses spaced about 10 units apart. We track the amplitude of the large pulse, which travels much faster than the equilibrium pulses, as a function of time in figure 4 for the subcritical conditions of $\delta = 0.6$ and 0.4. As is evident, the coalescence cascade still occurs for $\delta = 0.6$ even though the large pulse drains a significant amount of its liquid between coalescence events. As a result, its amplitude actually decreases in time despite the coalescence cascade. The drainage is so severe for $\delta = 0.4$ that the cascade stops after the first coalescence event. The large pulse has decayed into an equilibrium one after the first coalescence event and is unable to capture the next equilibrium pulse.

It is clear from the simulations that coalescence is driven by speed differential between pulses. For subcritical conditions, coalescence only occurs if there are excessively large pulses compared to the equilibrium ones. Even then, due to drainage from the large pulses, their amplitude can decay in time despite the fluid gain during coalescence and the coalescence cascade may not be sustainable. In constrast, drainage is always from the substrate to the pulse under supercritical conditions and this drainage amplifies the difference between pulses – it promotes coalescence.

3. Equilibrium subcritical pulses and stability

We shall demonstrate in this section that, in the absence of coalescence, a large non-equilibrium pulse (or any localized structure) will decay towards an equilibrium pulse under subcritical conditions and we shall estimate the decay rate by quantifying the fluid drainage rate from the pulse to the substrate. We do so by showing that the equilibrium pulses are linearly stable with a new spectral theory.

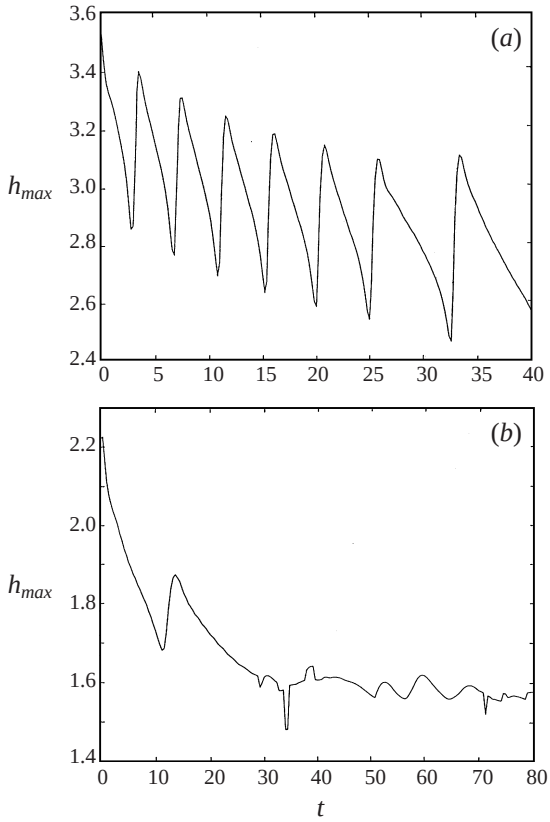

FIGURE 4. Amplitude of the large pulse (twice the equilibrium) behind a train of equilibrium pulses for (*a*) $\delta = 0.6$ and (*b*) 0.4.

Consider a single stationary pulse on a substrate of unit thickness (h_0 in the definition of δ is now taken to be the substrate thickness of a single pulse); these equilibrium pulses are defined by the following equations in a frame moving with constant speed c, a stationary version of (3):

$$\delta h_s^3 \left(\frac{\partial^3 h_s}{\partial x^3} + \frac{\partial h_s}{\partial x} \right) + \tfrac{2}{3} \left(h_s^3 - 1 \right) - c(h_s - 1) = 0, \tag{4a}$$

$$h_s(x \to \pm\, \infty) = 1. \tag{4b}$$

Construction of the stationary pulse then amounts to determining $c(\delta)$. Kalliadasis & Chang (1994*a*) showed by matched asymptotics that $c(\delta)$ blows up to infinity at the limiting δ value of δ_* such that equilibrium pulses only exist when δ is less than

$$\delta_* = 1.12 \tag{5}$$

which is a dimensionless version of (1). This corresponds to a substrate thickness thinner than h_c of (1). For $\delta < \delta_*$, each equilibrium pulse has the distinctive shape of a large pulse preceded by a deep dimple. As δ increases towards δ_*, the pulse becomes larger, the speed faster and the dimple curvature more pronounced until all three approach infinity at δ_*. Near δ_*, the speed c, amplitude h_s^{max} and area J of the

δ	c	J	h_s^{max}	$\lambda_\#$
0.1	2.152	0.316	1.095	−0.0137
0.2	2.304	0.634	1.191	−0.0267
0.3	2.521	1.061	1.321	−0.0388
0.4	2.809	1.603	1.488	−0.0496
0.5	3.205	2.314	1.707	−0.0592
0.6	3.781	3.289	2.012	−0.0668
0.7	4.687	4.714	2.458	−0.0738
0.8	6.279	6.997	3.175	−0.1000
0.85	7.606	8.746	3.728	−0.1510
0.9	9.645	11.240	4.516	−0.2510
0.95	13.020	14.990	5.701	−0.5670
1.0	18.900	20.790	7.544	−1.2200

TABLE 1. Properties of subcritical equilibrium pulses ($\delta < \delta_*$) with unit substrate

stationary pulses can be estimated as

$$c - 2 = \frac{2\delta^{2/3}}{\delta_*^{2/3} - \delta^{2/3}}, \tag{6a}$$

$$h_s^{max} - 1 = 0.371(c - 2), \tag{6b}$$

$$J = \int_{-\infty}^{\infty} (h_s - 1)\mathrm{d}x = 1.175(c - 2). \tag{6c}$$

Correlations (6) represent a slight empirical improvement of the analytical expressions derived by Kalliadasis & Chang near δ_* to extend the validity of the correlations further away from δ_*. We have also obtained the true values by constructing the stationary pulses numerically. These values are tabulated in table 1. As a check of their validity, we note that the decaying pulse in figure 4(*b*) approaches the equilibrium height of $h_{max} = 1.5$ in table 1 at $\delta = 0.4$. This again supports the observation that subcritical pulses decay towards the equilibrium pulses constructed from (4).

We linearize the evolution equation (3) about the pulse solution (4) to yield the linearized equation for the disturbance $u(x, t) = h(x, t) - h_s(x)$:

$$\frac{\partial u}{\partial t} = \mathrm{L}u, \tag{7}$$

where the linearized operator is

$$\mathrm{L} = -\frac{\partial}{\partial x}\left[\delta h_s^3 \left(\frac{\partial^3}{\partial x^3} + \frac{\partial}{\partial x}\right)\cdot + 3\delta h_s^2 \left(\frac{\mathrm{d}^3 h_s}{\mathrm{d}x^3} + \frac{\mathrm{d}h_s}{\mathrm{d}x}\right)\cdot + (2h_s^2 - c)\cdot\right]. \tag{8}$$

We shall restrict ourselves to bounded disturbances. As a result, all disturbances with finite mass (area), like the excess mass in a pulse, can be expanded in terms of the eigenfunctions ψ of the eigenvalue problem

$$\left.\begin{array}{c} \mathrm{L}\psi = \lambda\psi, \\ \psi \text{ bounded as } x \to \pm\infty. \end{array}\right\} \tag{9}$$

There are two kinds of eigenfunctions. Those eigenfunctions ψ_k that approach zero at infinite $|x|$ correspond to discrete eigenvalues λ_k. Since L is an exact differential, a simple integration of (9) shows that all discrete modes contain no mass, $\langle\psi_k\rangle =$

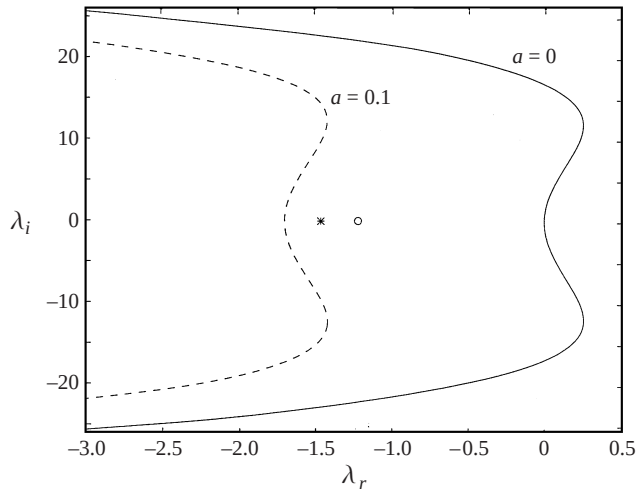

FIGURE 5. The spectrum of the equilibrium pulse at $\delta = 1$ in the complex λ-plane. The original and shifted essential spectra for indicated values of a are shown. The discrete eigenvalue is denoted by a star and the resonance pole an open circle. After the shift, the resonance pole becomes a discrete eigenvalue and the discrete eigenvalue a resonance pole. The former dominates the decay dynamics. The neutral eigenvalue, corresponding to translational symmetry, at the origin is not shown.

$\int_{-\infty}^{\infty} \psi_k \, \mathrm{d}x = 0$. This is a legacy of the gradient-flow form of the evolution equation (3) due to mass conservation. The eigenfunctions $\psi(\lambda, x) = K(\alpha, x)\mathrm{e}^{\mathrm{i}\alpha x}$ which approach bounded oscillations at the infinities belong to the essential spectrum defined by

$$\lambda(\alpha) = \mathrm{i}\alpha(c - 2) + \alpha^2\delta(1 - \alpha^2) \tag{10}$$

for $\alpha \in (0, \infty)$. The reason that (10) is simply the dispersion relationship for a flat film of unit thickness is because the equilibrium pulse decays into such a film at both infinities and the oscillations of the eigenfunctions must also be described by the flat-film dispersion relationship. There is a continuum of such 'radiation' modes since α takes all real values. Construction techniques for both the discrete and essential spectra are detailed in Chang, Demekhin & Kopelevich (1996) and Chang, Demekhin & Kalaidin (1998). We simply show a sample spectrum for the present operator in figure 5. Due to translational invariance, there is always a simple zero eigenvalue λ_1 at the origin that corresponds to the eigenfunction $\psi_0 = \mathrm{d}h_s/\mathrm{d}x$ (Chang *et al.* 1996). (This ever-existing neutral eigenvalue is not shown in the figure.) There is only one other discrete mode λ_2 that we could locate for the entire pulse family. It is always stable and is marked by an asterisk in figure 5 at the position of -1.463 for $\delta = 1$.

The essential spectrum shown in figure 5 seems to suggest that the stationary pulses are unstable. In fact, since none of the discrete modes carry mass, the mass draining from a decaying pulse must be carried by the continuum of the essential spectrum. Hence, the fact that the essential spectrum contains a band of unstable modes in the right-hand half of the complex plane seems to suggest a growing pulse and not a decaying pulse in drainage. Actually, the mass-carrying wavepackets spanned by the essential spectrum are of finite width and propagate at speeds different from the pulse. These wavepackets typically grow out of localized disturbances on substrates away from the pulse. On the flat substrate, the envelope $K(\alpha, x)$ of the essential eigenfunction approaches constant values and the eigenfunctions approach Fourier modes. Hence, the expansion coefficients of the essential eigenfunction for a

wavepacket on the substrate is simply the latter's Fourier coefficients and the unstable essential spectrum corresponds to the unstable Fourier modes within a wavepacket because the substrate is unstable. However, the growth of these unstable modes would only affect the pulse if the pulse cannot outrun the wavepacket – the pulse speed is slower than the group velocity. This is clearly not true from the pulse speed (6) and the substrate dispersion relationship (10). Hence, even if the growing wavepacket is initially in front of the pulse, it will be convected behind the pulse without affecting the stability of the pulse. When the wavepacket passes through the pulse, however, it will temporarily affect the pulse height before the absorbed mass carried by the wavepacket drains out of the pulse. Alternatively, the mass contained in a large pulse will drain out as a wavepacket as the pulse equilibrates. The wavepackets that drain out in both cases will grow on the substrate as the unstable Fourier modes extract energy from the Rayleigh instability. This growth, however, does not affect the pulse in front of the wavepacket.

Pego & Weinstein (1994) developed a weighted spectral theory to describe this convective stability of a pulse and we shall use it below to capture the equilibration rate towards a stationary pulse. A weighting function is placed on the disturbance u. This weight decays exponentially from the pulse in the direction of negative x in the moving frame. It hence suppresses the temporal growth of any wavepacket behind the pulse. Since localized disturbances in front of the pulse will eventually be convected behind the pulse, the weight does not introduce additional instability in front. Instead, it focuses on disturbances close to the pulse. If the pulse is unstable, the weighted disturbance will grow in time. If the pulse is stable, the weighted disturbance will decay in time. The drainage rate of excess fluid in a stable equilibrium pulse is then determined by the decay rate of the weighted disturbance. We hence use the e^{ax} weight of Pego & Weinstein on the disturbance u in (7), $v = \mathrm{e}^{ax}u$, and define a corresponding eigenvalue problem

$$\mathrm{L}_a\phi = \mathrm{e}^{ax}\mathrm{L}(\mathrm{e}^{-ax}\phi) = \lambda\phi, \tag{11}$$

where $\phi = \mathrm{e}^{ax}\psi$ is the weighted eigenfunction that spans the weighted disturbance $v(x,t)$.

It is clear that the essential spectrum Γ_a of L_a is related to that of L in (10) by the transformation $\alpha \to \alpha + \mathrm{i}a$:

$$\lambda_a = \mathrm{i}(\alpha + \mathrm{i}a)(c-2) + \delta(\alpha + \mathrm{i}a)^2[1 - (\alpha + \mathrm{i}a)^2]. \tag{12}$$

The net result is that the essential spectrum is shifted to the left in the complex plane. This is demonstrated in figure 5. The fact that a particular value of a exists that can shift the entire essential spectrum to the left-hand half-plane implies that the pulse is convectively stable – the weighted disturbance decays to zero in amplitude (Chang, Demekhin & Kopelevich 1995). Even though the drained mass will eventually grow on the trailing substrate, the pulse suffers no long-time perturbation locally. This is the essence of Pego & Weinstein's stability theory.

It can be shown (Chang *et al.* 1996) that, unlike the essential spectrum which is shifted by the weight, the discrete spectrum of L is also a discrete spectrum of L_a – with an important exception. The discrete eigenfunctions ψ_k of L decay to zero as $|x| \to \infty$ with an exponential rate determined by the roots α of the spatial characteristic polynomial

$$P(\alpha) = \lambda_k - \lambda(\alpha), \tag{13}$$

where λ_k is the discrete eigenvalue corresponding to ψ and $\lambda(\alpha)$ is given by the

dispersion relationship (10). The roots with positive real part determine the decay rate as $x \to -\infty$ and ones with negative real parts the rate as $x \to \infty$. However, one can, in principle, also construct functions which satisfy $L\psi_\# = \lambda_\# \psi_\#$ but do not decay to zero at one infinity. If, for example, there are two roots with negative real parts α_1 and α_2, $\psi_\#$ can decay to zero at $+\infty$ with rate α_1 but grow exponentially at $-\infty$ with rate α_2. Since the eigenfunctions $\psi_\#$ of these $\lambda_\#$ modes do not decay to zero, they are not part of the discrete spectrum and are called resonance poles (Pego & Weinstein, 1994). We have found only one real and negative resonance pole ($\lambda_\# < 0$) which is shown as an open circle in figure 5.

These resonance poles and their eigenfunctions also satisfy the weighted operator $L_a\phi_\# = \lambda_\#\phi_\#$ where $\phi_\# = \psi_\# e^{ax}$ but their asymptotic behaviour at $x \to \pm\infty$ can now change. Since the essential spectrum Γ_a for L_a is defined by $\lambda_a(\alpha)$ for α real, when there is a discrete eigenvalue on the essential spectrum Γ_a, one of the roots of the spatial characteristic polynomial (13) is purely imaginary. Consequently, as Γ_a is shifted across the resonance pole $\lambda_\#$, the negative root α_2 crosses the imaginary axis and its real part becomes positive. Hence, as Γ_a is shifted across the resonance pole, $\phi_\#$ now decays to zero at both infinities and the resonance pole becomes a discrete eigenvalue of L_a. Similarly, if Γ_a is shifted across the discrete eigenvalue λ_2, it becomes a resonance pole of L_a. The translational zero mode λ_1, as shown earlier by Chang *et al.* (1996), remains an eigenvalue as Γ_a passes by due to a hole in the Riemann surface defined by Γ_a. Other rules on the exchange between eigenvalues and resonance poles can be found in that reference. For all equilibrium pulses with $\delta < \delta_*$, we are able to shift Γ_a such that $\lambda_\#$ becomes a discrete eigenvalue of L_a and λ_2 a resonance pole as seen in figure 5. Hence, $\lambda_\#$ is the dominant mode of the weighted disturbance and it determines the asymptotic decay rate towards equilibrium pulses – the asymptotic drainage rate. The value of this resonance pole $\lambda_\#$ is tabulated in table 1. It becomes increasingly negative as δ approach δ_* from below. All equilibrium pulses are hence stable and all non-equilibrium pulses with a local substrate thinner than h_c are expected to decay into equilibrium pulses if they are not involved in further coalescence events. The decay rate $\lambda_\#$ increases with increasing substrate thickness.

To verify the decay rate estimated by the dominant resonance pole, we carry out a sequence of numerical studies with 'excited' lone pulses. The initial non-equilibrium pulse is $h(x, t = 0) = 1 + 1.2(h_s(x) - 1)$ in the frame moving at the equilibrium pulse speed c. This represents an added mass 20% of that carried by the equilibrium pulse. The drainage rate and the decay rate of the maxiumum pulse height h^{max} towards the equilibrium value should both be $\lambda_\#$ at large time, $h^{max} - h_s^{max} \sim 0.2(h_s^{max} - 1)e^{\lambda_\# t}$. We hence track $\eta(t) = t^{-1} \ln\left[h^{max}(t) - h_s^{max}/0.2(h_s^{max} - 1)\right]$ as the excited pulse decays. As seen in figure 6(*a*), $\eta(t)$ approaches a constant negative asymptotic value for $\delta < \delta_*$, indicating an exponential decay towards the equilibrium pulse. That large pulses decay rapidly towards equilibrium pulses under subcritical conditions explains why they do not evolve into drops. They cannot grow individually beyond the equilibrium pulse.

For $\delta < 0.8$, the asymptotic value of η is in excellent agreement with the resonance pole $\lambda_\#$ as seen in figure 6(*b*). For $0.8 < \delta < \delta_*$, however, oscillations are observed in $\eta(t)$ which become more pronounced as δ approaches δ_*. Some oscillations are evident in the $\delta = 0.9$ curve in figure 6(*a*). There seems to be an apparent equilibration of $\eta(t)$ as well but this asymptotic value deviates from the resonance pole $\lambda_\#$. The cause of the deviations of the resonance pole theory from the numerical results near δ_* is not at present understood.

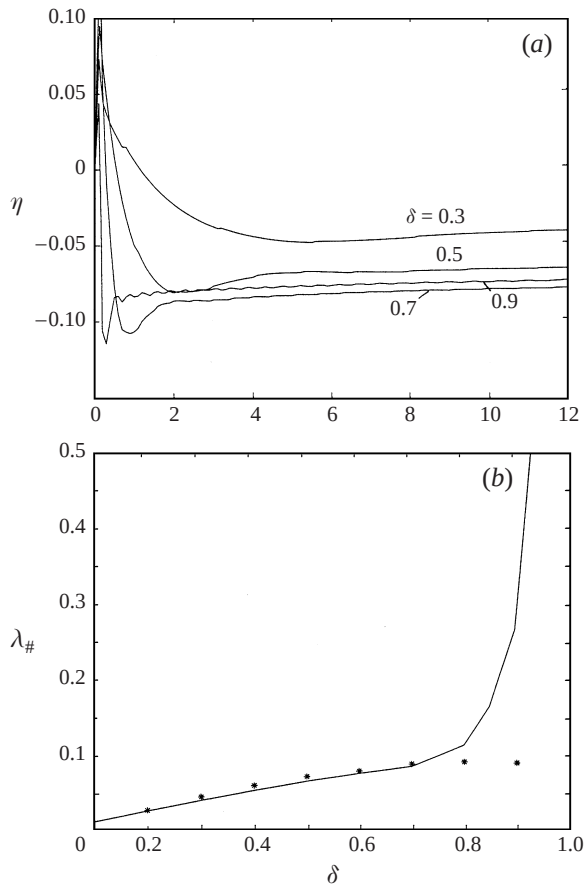

FIGURE 6. (*a*) The decay rate $\eta(t)$ from numerical simulation of how an 'excited' pulse with 20% added mass decays towards the equilibrium pulse for $\delta < 0.9$. (*b*) Comparison of the asymptotic decay rate $\eta(\infty)$ (asterisks) to the theoretical curve from the resonance poles.

4. Growth dynamics of supercritical pulses

When the local substrate thickness exceeds h_c, the corresponding δ is larger than δ_* of (5) and no stationary pulses exist. As a result, a local large structure cannot decay and approach an equilibrium pulse. To study its evolution towards a new asymptotic state, we place a large pulse of arbitrary shape on a unit substrate at $\delta = 1.5$ in figure 7. Soft boundary conditions are used instead of periodic boundary conditions for this large domain to ensure that a sufficiently large amount of liquid is available to fuel growth. A transient adjustment ensues over about 20 units of time. During this transient period, fluid is drained to the back of the pulse as it attempts to reach a non-existing equilibrium shape. It soon finds that a quasi-equilibrium position is possible only if the thickness of the back substrate layer, denoted $\chi(t)$ for convenience here, is smaller than the unit thickness in front. Due to this jump in substrate thickness across the pulse, the flow entering the pulse is larger than the exit value in the frame moving with the pulse and the pulse grows. The stationary equilibrium pulses for $\delta < \delta_*$ are hence replaced by growing pulses as the asymptotic states of localized structures for supercritical conditions, $\delta > \delta_*$. This growth by collecting liquid from the front substrate is a slow process compared to the local adjustment time for the interface. As

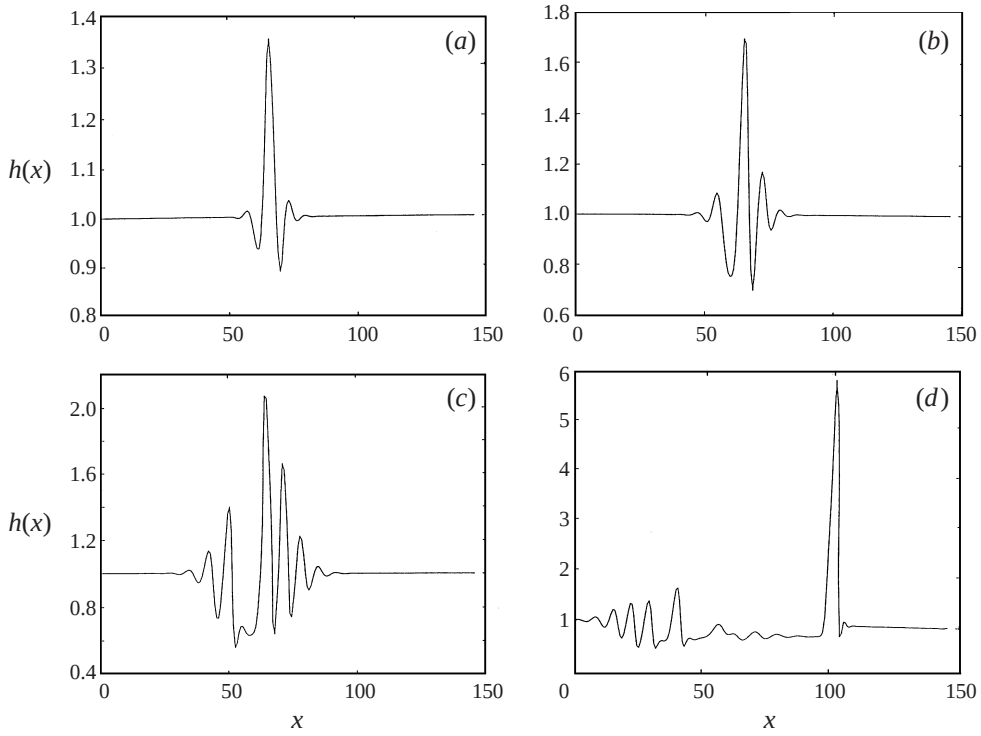

FIGURE 7. The transient for the formation of a growing pulse when a large pulse is placed on a unit substrate for $\delta = 1.5$. The snapshots are taken at t =2, 5, 10, and 20 (*a–d*). A quasi-steady jump in the substrate thickness is clearly evident by $t = 20$ after the transient wave packets convect away.

a result, the pulse and the inner regions connecting the pulse to the substrates remain quasi-static. The matched asymptotic analysis of Kalliadasis & Chang for stationary pulses can then be extended below to study this asymptotically growing pulse with a unique self-growth mechanism.

We shall divide the slowly-growing pulse into three regions and utilize matched asymptotics. The hydrostatic outer region at the peak of the growing pulse is expected to be dominated by azimuthal and axial capillary forces to leading order, with next-order corrections from gravity. To allow matched asymptotics, the quasi-steady pulse height must be large compared to the substrate thickness. For such large pulses, we expect the quasi-steady pulse speed c to also be large. We shall hence use $c^{-1/3}$ as the small parameter in the asymptotics. In the quasi-static outer region dominated by hydrostatics, the x scale is of unit order since the axial and azimuthal curvature terms h_x and h_{xxx} within the parentheses in (3) must balance. However, the pulse height h_{max} is large. As such, the curvature near the back of the pulse must be of order h_{max}. There are then the back inner region where the pulse meets the substrate layer of unit-order thickness χ and the front inner region where it meets the unit substrate thickness. Within both inner regions, one has the dominant Bretherton scaling which balances axial-curvature-driven flow $h^3 h_{xxx}$ with shear flow due to translation ch (Bretherton 1961). As such, the vertical length scale and the horizontal length scale must have a ratio of $h_x \sim O(c^{1/3})$. We know, however, from matching curvature with the outer region that $h_{xx} \sim O(h_{max})$ in the inner region. Since h is of unit order in both inner regions, we immediately conclude that $h_{max} \sim O(c^{2/3})$ in the outer region

and $x \sim O(c^{-1/3})$ in the inner regions. The dominant balances in all three regions do not involve the growth term $\partial/\partial t$ and this stipulates a relatively long time scale for slow growth.

To estimate the growth time scale, we integrate (3) from $x = -\infty$ where $h = \chi$ to $x = +\infty$ where $h = 1$ to yield a global mass balance over the jump

$$\frac{\partial}{\partial t}\int_{-\infty}^{+\infty} h\mathrm{d}x = c(1-\chi) - \tfrac{2}{3}(1-\chi^3) \sim c(1-\chi) \tag{14}$$

which yields a growth time of $O(c^{-1/3})$.

With $h \sim O(c^{2/3}), t \sim O(c^{-1/3})$ and $x \sim O(1)$ in the outer region, the evolution term $\partial h/\partial t$ in (3) is of negligible $O(c)$ compared to the dominant $O(c^{8/3}), O(c^2)$ and $O(c^{5/3})$ terms in (3). In fact, if we resolve the outer solution to the following order:

$$h \sim c^{2/3}(h_0 + c^{-1/3}h_1 + c^{-2/3}h_2 + \cdots) \tag{15}$$

the evolution term can be omitted – the outer solution is quasi-stationary.

Integrating (3) from $-\infty$ where $h = \chi$ and from $+\infty$ where $h = 1$, we get

$$\delta h^3(h_{xxx} + h_x) - c(h-\chi) + \tfrac{2}{3}(h^3 - \chi^3) + \frac{\partial}{\partial t}\int_{-\infty}^{x} h\mathrm{d}x = 0, \tag{16a}$$

$$\delta h^3(h_{xxx} + h_x) - c(h-1) + \tfrac{2}{3}(h^3 - 1) + \frac{\partial}{\partial t}\int_{x}^{+\infty} h\mathrm{d}x = 0. \tag{16b}$$

To leading orders of $O(c^{8/3})$ and $O(c^2)$, these two equations are identical,

$$\delta h^3(h_{xxx} + h_x) + \tfrac{2}{3}h^3 = O(c^{5/3}). \tag{17}$$

Substituting (15) into (17), we get

$$\frac{\mathrm{d}^3 h_0}{\mathrm{d}x^3} + \frac{\mathrm{d}h_0}{\mathrm{d}x} = 0, \tag{18a}$$

$$\frac{\mathrm{d}^3 h_1}{\mathrm{d}x^3} + \frac{\mathrm{d}h_1}{\mathrm{d}x} = 0, \tag{18b}$$

$$\frac{\mathrm{d}^3 h_2}{\mathrm{d}x^3} + \frac{\mathrm{d}h_2}{\mathrm{d}x} = -\frac{2}{3\delta}. \tag{18c}$$

The leading-order equation (18*a*) is just the long-wave Laplace–Young equation which possesses a static pulse solution symmetric about $x = \pi$:

$$h_0 = A'(t)(1 - \cos x). \tag{19}$$

This static solution has a constant width of 2π and makes contact with the substrate at $x = 0$ and 2π. With a non-trivial h_0, the next-order term h_1 vanishes exactly and the next non-trivial correction to the outer solution is

$$h_2 = -\frac{2}{3\delta}(x - \sin x) + B. \tag{20}$$

It elevates the substrate thickness to B at $x = 0$ and 2π and introduces an asymmetric correction to (19) after the baseline correction. The tilt forward is due to gravitational steepening in the $\frac{2}{3}h^3$ term in (16) and (17). Combining h_0 and h_2 and expanding about the contact points at the back $x = 0$ and at the front $z = x - 2\pi = 0$, we obtain

$$h(x \to 0) \sim A(t)\frac{x^2}{2} + B, \tag{21a}$$

$$h(z \to 0) \sim A(t)\frac{z^2}{2} + \left(B - \frac{4\pi}{3\delta}\right), \tag{21b}$$

where $A(t) = A'(t)c^{2/3}$.

In the two inner regions, we shall rescale the coordinates with the proper scales, $h \sim O(1)$ and $x \sim O(c^{-1/3})$. We shall also examine both sides at the same time and define the Bretherton variables

$$f = h/\chi, \quad \xi = \frac{1}{\chi}\left(\frac{c}{\delta}\right)^{1/3} x \tag{22}$$

such that $\chi = 1$ in front and $\chi \neq 1$ in the back. The rescaled (14) and (15) do not involve the dynamic term $(\partial/\partial t)(\cdot)$ to the leading three orders – the inner regions are also quasi-steady due to the small scales. In fact, only the dominant inner solution is required to match the outer expansion of (21). This the Bretherton equation (Bretherton 1961)

$$f_0''' - \frac{f_0 - 1}{f_0^3} = 0 \tag{23}$$

subject to the following boundary conditions at the two inner regions:

$$f_0 \to 1 \quad \text{as} \quad \xi \to \pm\infty \tag{24}$$

with the plus sign corresponding to the front inner region and minus to the back inner region.

Since the leading-order outer solution (19) is symmetric about $x = 0$ and makes tangential contact with the negligibly thin substrate, the two leading-order inner solutions must blow up quadratically to allow matching. In general, the asymptotic solutions of the Bretherton equation blow up with a vanishing third derivative and hence

$$f_0^{\pm}(\xi \to \pm\infty) \sim \alpha^{\pm}\xi^2 + \gamma^{\pm}\xi + \beta^{\pm}, \tag{25}$$

where $+$ denotes the behaviour of the back inner solution as ξ approaches $+\infty$ and $-$ denotes the asymptotic behaviour of the front inner solution at $-\infty$. There is also a possibility of a higher-order $\xi \ln \xi$ behaviour (Kalliadasis & Chang 1996) that can be matched with higher-order terms of (15). There is an additional degree of freedom in choosing the origin of ξ and this is chosen to suppress the linear $\gamma_{\pm}\xi$ term to ensure quadratic blow-up.

For the back inner region near $x = 0$, integrations by Bretherton (1961) and many others (see Kalliadasis & Chang 1994*a*, *b*, for example) show that there is only a unique asymptotic behaviour with

$$\alpha^+ = 0.32171, \quad \beta^+ = 2.898. \tag{26}$$

In the z-coordinate of the outer region, this corresponds to a unique inner asymptote for the back:

$$h^+ \sim \frac{\alpha^+}{\chi}\left(\frac{c}{\delta}\right)^{2/3} x^2 + \chi\beta^+, \quad x \to 0. \tag{27}$$

For the front inner region near $z = x - 2\pi = 0$, however, a family of inner asymptotes is now possible. One integrates the corresponding leading-order Bretherton equation (23) towards $\xi = -\infty$ with the initial condition

$$f_0 \sim 1 + \epsilon e^{-m\xi}\cos(n\xi + \theta), \tag{28}$$

where $m = 1/2$ and $n = 1/\sqrt{2}$. The parameters m and n correspond to the complex-conjugate eigenvalue pair for the flat-film dispersion relationship that grow as $\xi \to$

$-\infty$, namely $m > 0$. Because it is a complex pair, a phase θ enters the initial condition. For vanishingly small ϵ, integration of the Bretherton equation with (28) shows that a range of θ values yields quadratic asymptotic behaviour for f_0 at $\xi \to -\infty$. There is hence a family of (α^-, β^-) pairs which we shall represent in a functional form

$$\beta^- = \beta^-(\alpha^-). \tag{29}$$

The computed values of this function will be presented in a more convenient form later. In any case, a family of inner asymptotes exist for the front:

$$h^- \sim \alpha^- \left(\frac{c}{\delta}\right)^{2/3} z^2 + \beta^-, \quad z \to 0. \tag{30}$$

Baseline and curvature matching of the zeroth- and quadratic-order terms in the outer solution (21) to the inner asymptotes (27) and (30) yield four equations:

$$\frac{\alpha^+}{\chi}\left(\frac{c}{\delta}\right)^{2/3} = \frac{A}{2}, \quad \beta^+\chi = B, \tag{31a}$$

from matching at the back $x = 0$ and

$$\alpha^-\left(\frac{c}{\delta}\right)^{2/3} = \frac{A}{2}, \quad \beta^- = B - \frac{4\pi}{3\delta}, \tag{31b}$$

from matching at the front $x = 2\pi$. They allow us to eliminate the unknown B in the dominant outer terms and relate A, c, χ, δ and α^- by three relationships:

$$c = \left(\frac{A}{2\alpha^-}\right)^{3/2}\delta, \tag{32a}$$

$$\chi = \alpha^+/\alpha^-, \tag{32b}$$

$$\beta^- + \frac{4\pi}{3\delta} = \frac{\beta^+\alpha^+}{\alpha^-}, \tag{32c}$$

where β^- is a function α^-.

We note that at $\delta = \delta_* = 1.1201$, the solution to (32) is $\chi = 1, \alpha^- = \alpha^+ = 0.32171$ and $\beta^- = -0.8415$. This shows that the positive substrate jump vanishes at δ_* and reverses for $\delta < \delta_*$. Hence, the growing pulse solution exists only beyond δ_* where χ is less than unity. We can use (32c) to map the function $\beta^-(\alpha^-)$ into the functions $\beta^-(\delta)$ and $\alpha^-(\delta)$ in figure 8. From these relationships, we obtain how χ and c depend on δ from (32a) and (32b).

To get the drainage rate, we substitute the leading-order outer solution (19) into (14) and upon from $x = 0$ to 2π,

$$\frac{\mathrm{d}A}{\mathrm{d}t} \sim \frac{c(1-\chi)}{2\pi} = \kappa A^{3/2} \tag{33}$$

after substituting (32a), where the growth constant

$$\kappa = \frac{\delta(1-\chi)}{2\pi(2\alpha^-)^{3/2}} \tag{34}$$

is only a function of δ through (32b) and figure 8. This equation can be easily integrated to yield the blow-up behaviour of the growing pulse

$$A(t) = \frac{4}{\left(2(A(0))^{-1/2} - \kappa t\right)^2}. \tag{35}$$

The computed values of $\chi(\delta)$ and $\kappa(\delta)$ are shown in figure 9.

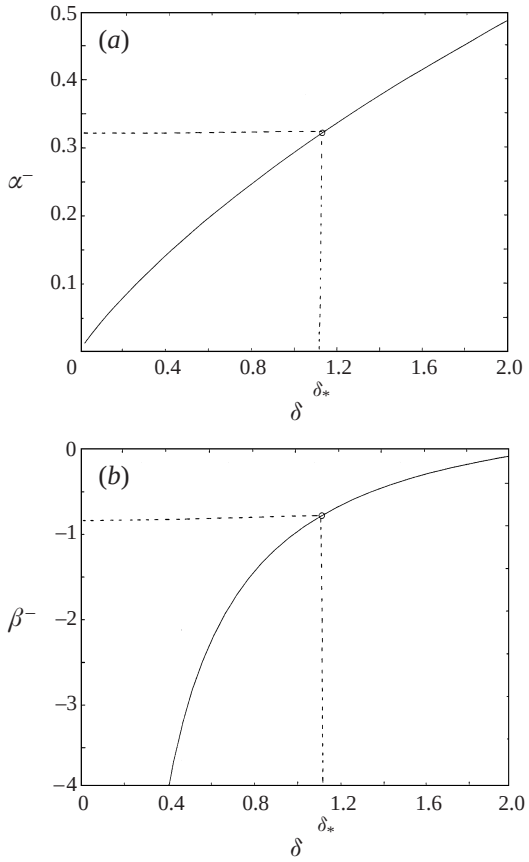

FIGURE 8. Dependence of α^- and β^- on δ from matched asymptotics. Even valves below δ_* are included.

It is then clear that the self-growth mechanism by using the substrate jump to collect liquid from the front substrate is only possible for $\delta > \delta_*(\kappa > 0)$. The blow-up time decreases with increasing $\delta - \delta_*$ and the blow up evolves in the manner described by (33) and (35). This blow-up behaviour is supported by the wave tracings of figure 10 where the large-time asymptotics of figure 7 are overlayed. The growth of the supercritical pulse is dramatically different from the decay of a subcritical pulse in figure 6(*a*). The asymptotic blow-up behaviour of (35) and (33) is confirmed in figure 11(*a*) by carrying out simulations for five values of $\delta > \delta_*$. The recorded trailing substrate thickness χ of the $\delta = 1.5$ case of figure 10 is shown in figure 11(*b*). The substrate thins rapidly during the pulse formation transient and slowly approaches the equilibrium value by $t = 10$ when the growing pulse is fully developed. The measured asymptotic $\chi(\delta)$ and $\kappa(\delta)$ values are favourably compared to the theoretical values of (34) and (32) in figure 9. Although the theory is developed for the growth dynamics of positive substrate jumps ($\chi < 1$), it seems to also capture the nonlinear decay dynamics towards equilibrium for δ between 0.8 and δ_*. This confirms the observation that the decay dynamics towards these large equilibrium pulses captured in figure 7 are actually transient nonlinear dynamics driven by finite-amplitude negative substrate jumps ($\chi > 1$). Unlike the growth dynamics that can proceed indefinitely with a large reservoir of liquid, the decay dynamics will eventually evolve into exponential decay.

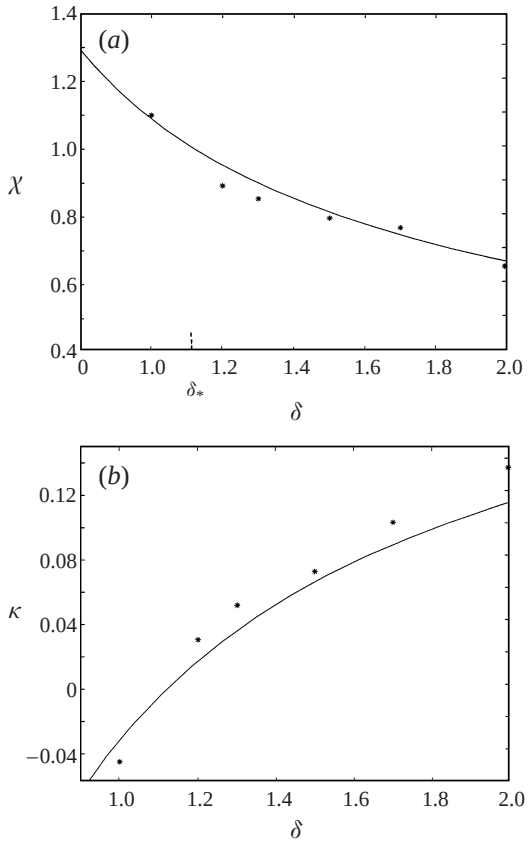

FIGURE 9. Measured χ and κ during the shock-driven growth of figures 10 and 11 compared to theoretical predictions of (32) and (34). The first data point is actually for a decaying pulse but the theory seems to still work.

The algebraic blow-up behaviour captured by (33) also indicates that the differential speed of two supercritical pulses blows up in time unless they are exactly the same amplitude. Hence, a large supercritical pulse will quickly outrun any smaller supercritical pulses in front. This explains the propensity of supercritical pulses to coalesce and the robustness of their coalescence cascades seen in figures 1 and 2.

5. Discussion

As is evident in figures 1 and 2(*b*), the substrate thickness thins monotonically in a finite periodic domain as liquid drains into the growing pulses. As a result, the growing pulses see a gradually thinning front substrate. The analysis of §4 is for a 'normalized' growing pulse with unit substrate thickness. We can renormalize the thinning substrate by realizing that (3) is invariant to

$$h \to h/\chi, \quad c \to c/\chi^2, \quad \delta \to \delta\chi, \quad x \to x, \quad t \to \chi^2 t, \tag{36}$$

where χ now refers to the thickness of the front substrate. Consequently, the effective δ for the growing pulse is $\delta\chi$. For an initially supercritical film, (36) indicates that as $\delta\chi$ approaches δ_*, the pulse stops growing and front and trailing substrates equilibrate

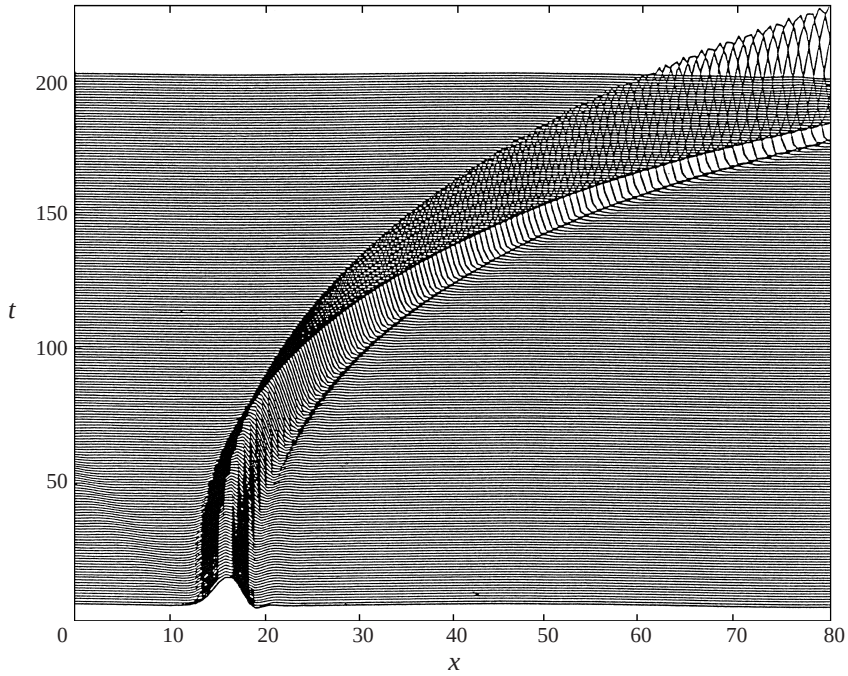

FIGURE 10. Large-time self-similar blow-up of the pulse in figure 7.

to the same equilibrium value of

$$\chi_{eq} = \delta_*/\delta. \tag{37}$$

This equilibrium substrate is clearly approached in our supercritical simulations of figures 1 and 2 with random initial conditions. After the coalescence cascade, only one supercritical pulse remains and it grows until the front substrate that feeds it thins to χ_{eq}, as seen in figure 2(*b*).

The growth also stops at $\chi = \chi_{eq}$ when there are multiple supercritical pulses provided they have ceased to interact and coalesce. Kerchman & Frenkel have carried out extensive supercritical simulations on a periodic domain with random initial conditions. We reproduce their recorded range of substrate thickness at the end of their simulations in figure 12. In some cases, there remain multiple pulses at the end that continue to interact and coalesce. Nevertheless, the upper bound of their band of equilibrium substrate thickness is closely approximated by (37), as seen in figure 12. The recorded lower equilibrium values suggest there are patches of subcritical equilibrium pulses on thinner substrates other than the supercritical growing pulses.

It must be recognized that the cessation of pulse growth at χ_{eq} is due entirely to our finite periodic computation domain. The final growing pulse in figure 1 actually returns around the domain and drains its own substrate. On a real fibre, pulses grow down the fibre and a growing pulse would sustain the same χ as it moves down. Whether growing pulses would develop then depends on the substrate thickness h_f at the point where the dimpled pulses first form from the initial non-stationary waves, as in figure 1(*b*). This thickness is smaller than the original waveless value h_0 due to drainage into the infant pulses. If h_f is smaller than h_c, the pulses will equilibrate into stationary subcritical pulses and if it exceeds h_c, growing pulses will form and develop into drops by coalescence and by collecting liquid from the substrate.

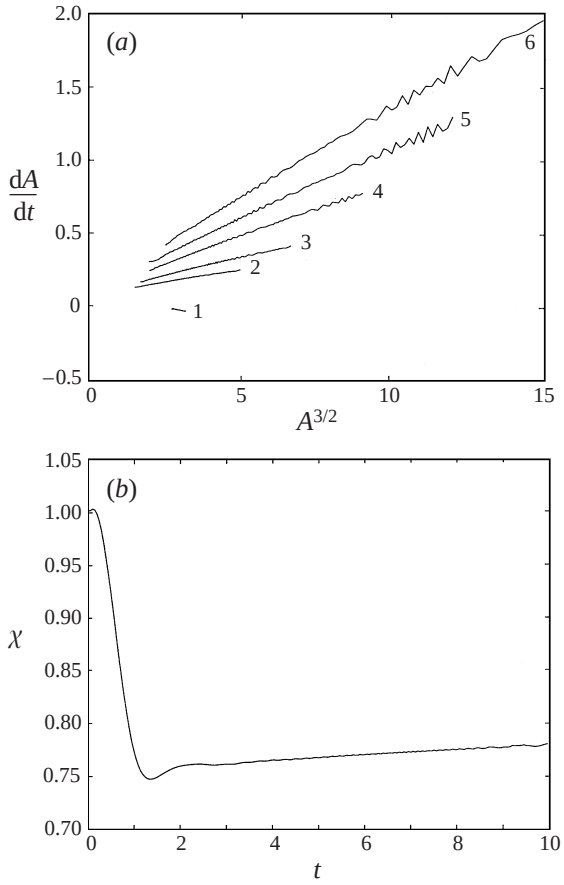

FIGURE 11. (*a*) The self-similar blow-up of the amplitude of a growing pulse sucking liquid from the front substrate driven by the shock. The growth rate of the pulse amplitude A relative to the mean thickness $\mathrm{d}A/\mathrm{d}t$ is shown to be linear with respect to $A^{3/2}$ during the growth for $\delta = 1.0$, 1.2, 1.3, 1.5, 1.7, and 2 (curves 1 to 6). The first curve breaks the correlation since this pulse actually decays as $\delta < \delta_*$. (*b*) Approach to an equilibrium trailing substrate thickness for the $\delta = 1.5$ case in figure 7.

Since h_f is smaller than h_0, it is clear that if h_0 is smaller than h_c, drops will not form. It is not as clear whether drops will form if h_0 is above h_c. The value of h_f is dependent on the pulse density at formation and hence sensitive to the initial conditions. Simulations by Kerchman & Frenkel indicate that, for h_0 slightly in excess of h_c, growing supercritical pulses or saturated subcritical pulses are equally likely as the final outcome. It is not until h_0 exceeds $3h_c$ that coalescence cascades driven by growing pulses always form from small-amplitude random initial conditions. This is also seen in figure 1 where h_f in figure 1(*b*) is about 1/3 the initial thickness. There is hence a band of initial wave thickness, $h_c < h_0 < 3h_c$, from which drop formation is possible but can only be induced with large and localized perturbations which produce a low pulse density at the formation stage. We suspect that Quere's experimental condition introduces such perturbations rather than small-amplitude random noise. This would explain why his measured critical h_0 is so close to h_c.

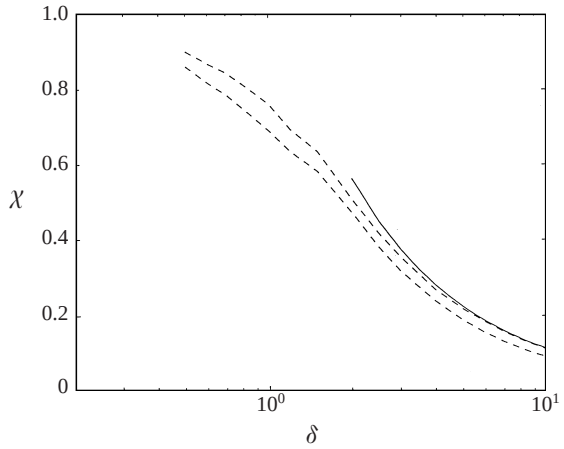

FIGURE 12. The predicted equilibrium substrate thickness with random initial noise at slightly supercritical conditions ($\delta > \delta_*$) as a function of δ (solid curve). The dotted curves bound the measured values from Kerchman & Frenkel's various simulations. The theory obviously is not appropriate for $\delta < \delta_*$.

Appendix. Regularized equations

The evolution equation (3) is derived from a leading-order lubrication expansion in $\epsilon = h_0/R$. The dimensionless radial position, scaled with respect to R, is $1 + \epsilon h$ where h is scaled with respect to h_0. The theory requires ϵh to be small which is questionable for very large pulses and for equilibrium pulses near δ_*. (The simplification involves a long-wave expansion of the curvature as well as other terms.) It is hence desirable to improve the resolution of (3). Unfortunately, there is currently no rigorous way of extending the lubrication equation to higher orders and one must resort to non-rigorous 'regularized' models that include the full curvature (Gauglitz & Radke 1988; Ratulowski & Chang 1989; Johnson *et al.* 1991; Halpern & Grotberg 1993). In the lens formation problem studied by those workers, the rigorous lubrication equation of Hammond (1983), analogous to (3), fails to capture the lens formation dynamics while the *ad hoc* regularized equation reproduces it faithfully. It is hence believed that the latter equation provides a reasonable extension of the former. We shall hence also examine our theory with the 'regularized' version of (3),

$$\frac{\partial h}{\partial t} = \frac{1}{1+\epsilon h}\frac{\partial}{\partial x}\left(\delta h^3 \frac{\partial K}{\partial x} - \tfrac{2}{3}h^3 - ch\right),$$

where K is the full curvature

$$K = -\frac{h_{xx}}{(1+\epsilon^2 h_x^2)^{3/2}} + \frac{\epsilon^{-1}}{(1+\epsilon h)(1+\epsilon^2 h_x^2)^{1/2}}.$$

It is clear that the above equation approaches (3) in the limit of vanishing ϵ.

The equilibrium pulses of (3) have infinite amplitude as δ approaches δ_* and it is here where the lubrication approximation is least accurate. We have constructed the stationary pulse solutions of the regularized equation and, as seen in figure 13, the critical δ_* vanishes for finite ϵ and stationary pulse solutions exist for all ϵ. However, for sufficiently small ϵ, the amplitude h_{max} of the pulses is well approximated by (3) even as it begins to diverge near δ_*. It is only very close to δ_* and for very large pulses that h_{max} of the regularized pulses ceases to diverge and begins to flatten with

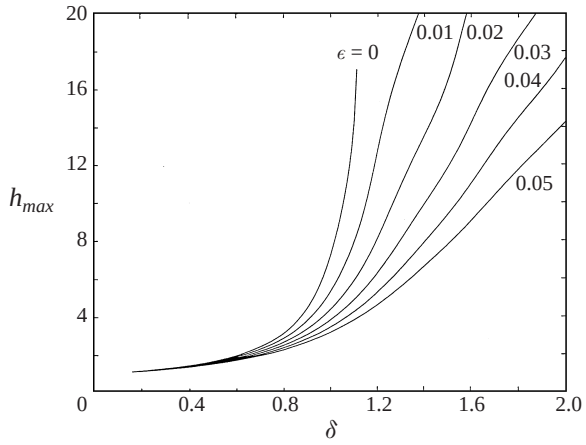

FIGURE 13. Equilibrium pulse amplitude $h_s^{max}(\delta, \epsilon)$ for the regularized equation.

respect to δ. Such regularized pulses beyond δ_* are exceedingly large but their ϵh remains small – a consequence of the regularization. They can be considered as drops in practice although they may not have the correct shape due to the uncertainties involved in the *ad hoc* regularization

Our transient simulation with the regularized equation indicates that any pulse growth will eventually be saturated if there is sufficient liquid for the pulses to absorb to grow into these large regularized pulses. However, the coalescence and self-similar growth prior to saturation at these large pulses are essentially identical to the self-similar blow-up of (3) if ϵ is sufficiently small. For larger values of ϵ, however, any growth mechanism beyond δ_* will be suppressed almost immediately by these regularized pulses. This suggests that drop formation can only occur for a sufficiently small $\epsilon < 0.01$. Returning to the critical condition $h_0 < h_c = 1.68R^3H^{-2}$, this constraint implies that the fibre radius must be smaller than one-tenth of the capillary length H. This is consistent with Quere's observation: drops do not form on large fibres. Due to the similarity between the evolution of (3) and the regularized equation, except near the drop-like regularized waves for $\delta > \delta_*$, we shall use (3) for our studies for a sufficiently small ϵ. This eliminates one parameter from consideration and the non-existence of equilibrium pulses beyond δ_* allows a matched asymptotic analysis of the self-similar blow-up asymptotics in § 4.

This work is supported by a NASA grant and an NSF grant. We are grateful to a reviewer for observations which significantly generalized the growth analysis.

REFERENCES

BRETHERTON, F. P. 1961 The motion of long bubbles in tubes. *J. Fluid Mech.* **10**, 166–188.

CHANG, H.-C., DEMEKHIN, E. A. & KALAIDIN, E. 1998 Generation and suppression of radiation by solitary pulses *SIAM J. Appl. Maths* **58**, 1246–1277.

CHANG, H.-C., DEMEKHIN, E. A. & KOPELEVICH, D. I. 1995 Stability of a solitary pulse against wave packet disturbance in an active medium. *Phys. Rev. Lett.* **75**, 1747–1750.

CHANG, H.-C., DEMEKHIN, E. A. & KOPELEVICH, D. I. 1996 Local stability theory of solitary pulses in an active medium. *Physica* D **97**, 353–375.

CHANG, H.-C., DEMEKHIN, E. A., KOPELEVICH, D. I. & YE, Y. 1997 Nonlinear wavenumber selection in gradient-flow systems. *Phys. Rev.* E **55**, 2818–2828.

Frenkel, A. L. 1992 Nonlinear theory of strongly undulating thin films flowing down vertical cylinders. *Europhys. Lett.* **18**, 583–588.

Gauglitz, P. A. & Radke, C. J. 1988 An extended evolution equation for liquid film breakup in cylindrical capillaries. *Chem Engng Sci.* **43**, 1457–1465.

Halpern, D. & Grotberg, J. B. 1993 Surfactant effects on fluid-elastic instabilities of liquid-lined flexible tubes: a model of airway closure. *J. Biomed. Engng* **115**, 271–277.

Hammond, P. S. 1983 Nonlinear adjustment of a thin annular film of viscous fluid surrounding a thread of another within a circular cylindrical pipe. *J. Fluid Mech.* **137**, 363–384.

Johnson, M., Kamm, R., Ho, L. W., Shapiro, A. & Pedley, T. J. 1991 The nonlinear growth of surface-tension driven instabilities of a thin annular film. *J. Fluid Mech.* **233**, 141–156.

Kalliadasis, S. & Chang, H.-C. 1994*a* Drop formation during coating of vertical fibres. *J. Fluid Mech.* **261**, 135–168.

Kalliadasis, S. & Chang, H.-C. 1994*b* Apparent dynamic contact angle of an advancing gas-liquid meniscus. *Phys. Fluids* **6**, 12–23.

Kalliadasis, S. & Chang, H.-C. 1996 Effects of wettability on spreading dynamics. *Ind. Engng Chem. Fundam.* **35**, 2860–2874.

Kerchman, V. I. & Frenkel, A. L. 1994 Interactions of coherent structures in a film flow: simulations of a highly nonlinear evolution equation. *Theor. Comput. Fluid Dyn.* **6**, 235–254.

Pego, R. L. & Weinstein, M. I. 1994 Asymptotic stability of solitary waves. *Commun. Math. Phys.* **164**, 305–350.

Quere, D. 1990 Thin films flowing on vertical fibres. *Europhys. Lett.* **13**, 721–726.

Ratulowski, J. & Chang, H.-C. 1989 Transport of gas bubbles in capillaries. *Phys. Fluids* A **1**, 1642–1655.

Trifonov, Yu. Ya. 1992 Steady-state traveling on the surface of a viscous liquid film falling down on vertical wires and tubes. *AIChE J.* **38**, 821–834.

Wilson, S. D. R. 1982 The drag-out problem in film coating theory. *J. Engng Maths* **16**, 209–221.

Wilson, S. D. R. & Jones, A. F. 1983 The entry of a falling film into a pool and the air entrainment problem. *J. Fluid Mech.* **128**, 219–230.